MHD Energy Bypass Scramjet Performance With Real Gas Effects

Chul Park*

ELORET Corporation, Sunnyvale, CA 94087

Unmeel B. Mehta+

NASA Ames Research Center, Moffett Field, CA 94035

and

David W. Bogdanoff×

ELORET Corporation, Sunnyvale, CA 94087

Abstract

*Senior Research Scientist; Fellow, AIAA; e-mail: cpark@mail.arc.nasa.gov; mailing address: Mail Stop 229-1, NASA Ames Research Center, Moffett Field, CA 94035.

+Division Scientist, Space Technology Division; Associate Fellow, AIAA; e-mail: umehta@mail.arc.nasa.gov; mailing address: Mail Stop T27B, NASA Ames Research Center, Moffett Field, CA 94035.

×Senior Research Scientist; Associate Fellow, AIAA; e-mail: dbogdanoff@mail.arc.nasa.gov; mailing address: Mail Stop 230-2, NASA Ames Research Center, Moffett Field, CA 94035.

The theoretical performance of a scramjet propulsion system incorporating an magneto-hydro-dynamic (MHD) energy bypass scheme is calculated. The one-dimensional analysis developed earlier, in which the theoretical performance is calculated neglecting skin friction and using a sudden-freezing approximation for the nozzle flow, is modified to incorporate the method of Van Driest for turbulent skin friction and a finite-rate chemistry calculation in the nozzle. Unlike in the earlier design, in which four ramp compressions occurred in the pitch plane, in the present design the first two ramp compressions occur in the pitch plane and the next two compressions occur in the yaw plane. The results for the simplified design of a spaceliner show that (1) the present design produces higher specific impulses than the earlier design, (2) skin friction substantially reduces thrust and specific impulse, and (3) the specific impulse of the MHD-bypass system is still better than the non-MHD system and typical rocket over a narrow region of flight speeds and design parameters. Results suggest that the energy management with MHD principles offers the possibility of improving the performance of the scramjet. The technical issues needing further studies are identified.

Nomenclature

B: Magnetic field strength, Tesla.

E: Electric field strength, V/m.

H: Height of vehicle, m.

h: Reactor entrance height/width, m.

M_c: Combustor entrance Mach number

P: Pitch (Fig. 3).

T: Temperature, K.

x: Axial distance, m.

y: Lateral distance, m.

u: Axial velocity, m/s.

V: Flight velocity, m/s.

α_1: Load factor (E_y/uB) for generator.

α_2: Load factor (E_y/uB) for accelerator.

δ: Boundary layer momentum thickness, m.

θ: Ramp angle, deg.

Introduction

In a scramjet propulsion system, one well-known difficulty is the fact that combustion is inefficient in the combustor when the Mach number of the airflow entering the combustor is high. In Refs. 1-3, it was noted that energy management with magneto-hydro-dynamic (MHD) techniques present a possible means for extending the flight Mach number envelope of conventional engines. This idea can also be used to improve the performance of the scramjet combustor by the use of the MHD principles.[4] In the proposal, the flow entering the combustor is to be decelerated by the use of an MHD generator. The electrical energy extracted from the MHD generator is expended to accelerate the flow by the use of an MHD accelerator after the combustion and prior to entering the nozzle expansion.

In Refs. 4 and 5, the theoretical performance of such an MHD-energy bypass scramjet propulsion system is calculated under several simplifying assumptions. The most important of those assumptions are that: 1) the flow is inviscid and therefore no friction drag is produced, 2) the chemical reactions in the expanding nozzle undergo freezing suddenly, and 3) inlet compression occurs by four ramp compressions in the pitch plane. The calculation presents an envelope of specific impulse values attainable with such a system under these assumptions, and compares it with those for a non-MHD scramjet system. The comparison shows that, in the flight speed range from about 3.4 to 4 km/s, the MHD-bypass system produces specific impulses higher than the non-MHD system and a typical rocket.

In the present work, the earlier method of performance calculation is improved. The flow is taken to be viscous, and the chemical reactions occur at a finite rate. The first two ramp compressions occur in the pitch plane, but the next two ramp compressions occur in the yaw plane. Other assumptions used in Ref. 4, such as ideal one-dimensional performance of the MHD devices, are retained in the present work.

The results show that finite-rate chemistry produces nearly the same results as the sudden-freezing approximation, the new geometry produces generally larger specific impulse, but the friction substantially reduces specific impulse. However, compared with the non-MHD system, the MHD-bypass system is still superior at a speed range above 3.4 km/s under certain restrictions on the geometry. The areas needing further research and development are identified.

Method

Two-Plane Four-ramp Design

In an idealized scramjet system, the compression of the air flow entering the combustion chamber is achieved through the use of a curved ramp, which compresses air through a nearly isentropic process to an angle typically of about 15 degrees. At the end of this compression, the flow is turned abruptly in the inlet of the engine so that the flow becomes approximately parallel to the oncoming free stream. The flow then enters an isolator wherein the flow passes through multiple weak shock waves. The isolator isolates the effect of combustion-induced disturbances on inlet operation. The flow is generally three-dimensional. The combustor following the isolator is usually relatively long, because a long distance is needed in order for the flow to complete combustion at high supersonic or hypersonic speeds.

In Ref. 4, this complex compression process is approximately represented by a simple four-ramp system. In that representation, the flow makes four turns of a same specified angle within the pitch plane, as shown schematically in Fig. 1. This design will be referred to hereafter as single-plane four-ramp compression design. In this design, the flow entering the reactor (MHD generator + combustor + MHD accelerator) has a laterally elongated cross section: the width spans the entire vehicle and the height is only about few centimeters. In an inviscid calculation, this elongated cross-section had no consequences.

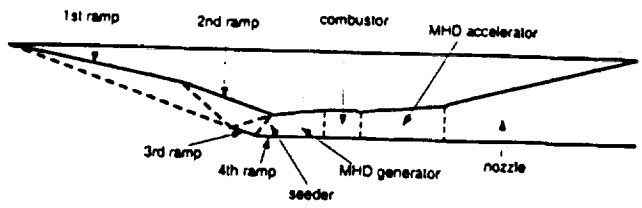

Figure 1. Quasi-one-dimensional single-plane four-ramp compression inlet system.[4]

The skin friction inside such an elongated reactor becomes large because the geometry produces a large wetted surfaced area. In order to reduce the skin friction to the minimum, the wetted area inside the reactor must be kept to the minimum. The minimum wetted area is obtainable with a square cross section. When other design factors are considered, a square cross section could be non-optimum or inappropriate.

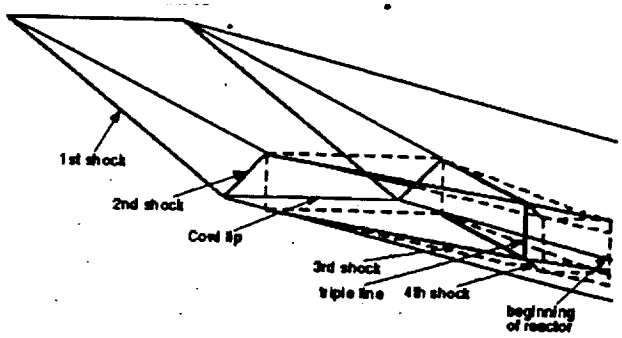

Figure 2. A schematic of two-plane four-ramp compression inlet system with shock patterns.

As in the single-plane four-ramp design, all turn angles are assumed to be equal. The consequences of deviating from this assumption are discussed later. The first two turns are made within the pitch plane, but the next two turns are made within the yaw plane, as shown schematically in Figs. 2 and 3. The lengths of ramps are specified in this model such that, at the end of the four-step compression, the cross-section of the flow path is a square. The dimensions of the design are uniquely determined by specifying the common

ramp angle θ and the height of the vehicle H (see Fig. 3). The overall length of the vehicle is fixed at 46 m. Of particular interest is the pitch, P, and the width and height of the reactor at its entrance, h (see Fig. 3). This design is termed two-plane four-ramp compression design. The scramjet vehicle employing such a four-ramp system is shown schematically in Fig. 4. Several of those engine units are ganged laterally.

In Fig. 5, the reactor is shown schematically for both non-MHD and MHD-bypass systems. For a non-MHD system, the reactor consists of an isolator, a fuel injector, and a combustor. For an MHD-energy bypass system, the isolator must function also as a seeder and an MHD power generator. A fuel injector must follow the MHD generator. The combustor, connected to the fuel injector, must function also as an MHD accelerator. The lengths of these components are chosen arbitrarily as shown in Fig. 5 for the present work. The cross-section is assumed to be always a square. The dimensions of the square vary slightly for the MHD case as shown schematically, because of the increase in entropy due to Joule heating and because of the flow acceleration.

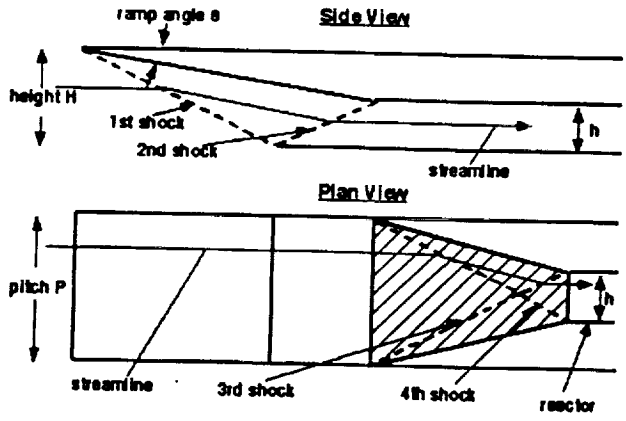

Figure 3. Flow path in the two-plane four-ramp compression inlet system.

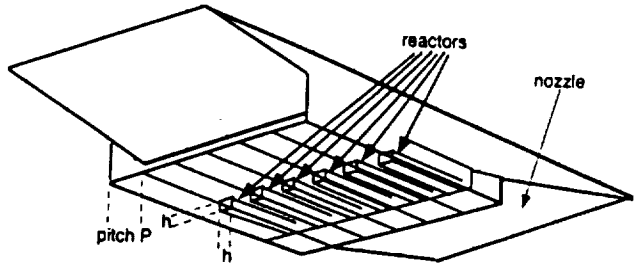

Figure 4. Schematic view of a scramjet vehicle employing two-plane four-ramp inlet system.

Inviscid Calculation Along Flow Path

As in Ref. 4, the flow properties are assumed to be in equilibrium up until the point in the nozzle at which chemical freezing takes place. In the MHD generator and accelerator, the flow is assumed to be uniform across the cross section; and the ideal one-dimensional MHD equations, given in Ref. 4, are assumed to be valid. The parameter dictating the design of the MHD devices is the load factor $\alpha = E_y/uB$. This parameter, the dimension of the entrance of the MHD device (h for the generator and the corresponding dimension for the accelerator, see Fig. 3), and the requirement that the MHD action be completed at the end of the given length of the MHD device completely specify the design of the MHD devices including the magnetic field strength B, electrical field strength in the lateral and axial directions, E_y and E_x, electrical current, and the Hall parameter.

At the end of the fourth compression, seeding is assumed to occur. Liquid potassium or cesium is assumed to be injected into the flow instantly without causing shock waves or viscous dissipation. The flow exiting from the MHD generator enters the combustion chamber. Here, gaseous hydrogen fuel is assumed to be mixed instantly without causing any shock waves or viscous dissipation.

In Ref. 4, the mass fraction of the seed substance was varied. The specific impulse was found to be only mildly dependent on the seed mass fraction. The optimum values of mass fraction were found to be about 0.001 for potassium and 0.003 for cesium by mass. These values are assumed in the present work throughout. The method of fuel injection is described in Ref. 4.

For the purpose of calculating the inviscid flow properties, the expansion following the MHD accelerator is assumed to occur with a linearly increasing cross-sectional area. The rate of increase of the cross-sectional area is chosen so that, at the end of the expansion, the height of the nozzle equals the height of the vehicle, as indicated in Fig. 4.

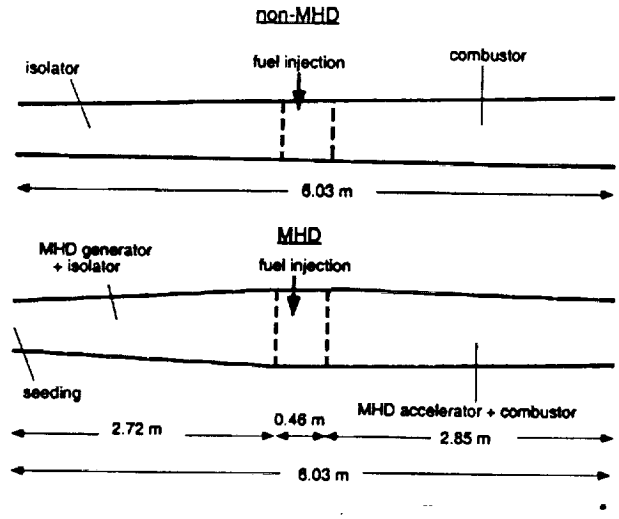

Figure 5. Schematic of the reactor.

In Ref. 4, the flow properties are calculated for the expansion region using a sudden-freezing approximation. In the present work, this is replaced by a finite-rate kinetic calculation. The chemical species considered are O, N, H, O_2, N_2, H_2, NO, OH, H_2O, and a seed substance, its ions, and electrons. The seed substance is potassium, K, or cesium, Cs. The forward (endothermic) reaction rates are expressed as

$$k = AT^n e^{-Tr/T} \text{ cm}^3/(\text{mol-s}).$$

The parameters A, n, and Tr are obtained from Refs. 6 to 9. They are summarized in Table 1.

Table 1. Reaction rates used. A is in the units of cm^3/(mol-s). M is the third body.

M	A	n	Tr	Reference
(1) $H_2 + M \rightarrow H + H + M$				
O	2.940e 18	-1.0	52500	Baulch et al[7]
N	2.940e 18	-1.0	52500	Baulch et al[7]
H	2.940e 18	-1.0	52500	Baulch et al[7]
K/Cs	2.940e 18	-1.0	52500	Baulch et al[7]
O_2	2.940e 18	-1.0	52500	Baulch et al[7]
N2	2.940e 18	-1.0	52500	Baulch et al[7]
H_2	7.350e 18	-1.0	52500	Baulch et al[7]
NO	2.940e 18	-1.0	52500	Baulch et al[7]
OH	2.940e 18	-1.0	52500	Baulch et al[7]
H_2O	4.780e 19	-1.0	52500	NASP cmt.[8]
K^+/Cs^+	2.940e 18	-1.0	52500	Baulch et al[7]
(2) $O_2 + M \rightarrow O + O + M$				
O	5.090e 18	-1.1	59360	Park[6]
N	5.090e 18	-1.1	59360	Park[6]
H	5.090e 18	-1.1	59360	Park[6]
K/Cs	5.090e 18	-1.1	59360	Park[6]
O_2	5.090e 18	-1.1	59360	Park[6]
N2	5.090e 18	-1.1	59360	Park[6]
H_2	2.000e 18	-1.1	59360	Park[6]
NO	1.270e 19	-1.1	59360	Park[6]
OH	5.090e 18	-1.1	59360	Park[6]
H_2O	8.270e 19	-1.1	59360	Park[6]

K^+/Cs^+	5.090e 18	-1.1	59360	Park[6]

(3) $OH + M \rightarrow + H +$ M

O	2.400e 13	0.3	5000	Baulch et al[7]
N	2.400e 13	0.3	5000	Baulch et al[7]
H	2.400e 13	0.3	5000	Baulch et al[7]
K/Cs	2.400e 13	0.3	5000	Baulch et al[7]
O_2	2.400e 13	0.3	5000	Baulch et al[7]
N2	2.400e 13	0.3	5000	Baulch et al[7]
H_2	6.000e 13	0.3	5000	Baulch et al[7]
NO	2.400e 13	0.3	5000	Baulch et al[7]
OH	2.400e 13	0.3	5000	Baulch et al[7]
H_2O	3.900e 14	0.3	5000	Baulch et al[7]
K^+/Cs^+	2.400e 13	0.3	5000	Baulch et al[7]

(4) $H_2O +$ M $\rightarrow$ OH + H + M

O	1.060e 25	-2.5	61000	Baulch et al[7]
N	1.060e 25	-2.5	61000	Baulch et al[7]
H	1.060e 25	-2.5	61000	Baulch et al[7]
K/Cs	1.060e 25	-2.5	61000	Baulch et al[7]
O_2	1.060e 25	-2.5	61000	Baulch et al[7]
N2	1.060e 25	-2.5	61000	Baulch et al[7]
H_2	2.650e 25	-2.5	61000	Baulch et al[7]
NO	1.060e 25	-2.5	61000	Baulch et al[7]
OH	1.060e 25	-2.5	61000	Baulch et al[7]
H_2O	1.720e 26	-2.5	61000	Baulch et al[7]
K^+/Cs^+	1.060e 25	-2.5	61000	Baulch et al[7]

(4) $K + e^- \rightarrow K^+ + e^- + e^-$

3.900e 33 -3.78 45180 Park[6]

(4) $Cs + e^- \rightarrow Cs^+ + e^- + e^-$

3.900e 33 -3.78 45180 Park[6]

(5) $N_2 + O \rightarrow NO + N$

5.690e 12 0.42 42938 Bose et al[9]

(6) $O + NO \rightarrow N + O_2$

2.360e 9 1.00 19220 Park[6]

(7) $H_2O + H \rightarrow H_2 + OH$

2.760e 10 1.12 10250 Baulch et al[7]

(8) $H_2 + O \rightarrow H + OH$

5.060e 4 2.67 3166 Baulch et al[7]

(8) $O_2 + H \rightarrow OH + O$

1.910e 14 0. 8273 Baulch et al[7]

Skin Friction

The boundary layer flow along the wall in the flow path is assumed to be fully turbulent. Van Driest equations[10,11] for fully turbulent flow over a flat plate are used to calculate the skin friction. These equations yield the skin friction over a flat plate between the given distances x_1 and x_2 away from the sharp leading edge. At x_1, the equations yield also the boundary layer momentum thickness δ_1. The thickness δ_1 can be used interchangeably to denote the distance x_1. This relationship between δ_1, rather than x_1, and skin friction is made into a routine in the present work.

This routine is then used in calculating the friction over a curved surface or a flat surface with varying flow conditions. The surface is divided first into small segments of length $\Delta x = x_2 - x_1 = 0.05$ m. At the apex of the vehicle or the leading edge of the cowl (i.e. the second ramp, see Fig. 3), δ is zero. Over each Δx, the flow properties at the edge of the boundary layer are assumed to be unchanged. Then, using the routine, the

friction over that segment is calculated. The calculation yields the δ value at the exit of this segment, δ_2. This δ_2 value is used in the calculation for the next segment, and so on.

In the region of the third ramp (the hatched area in the bottom figure in Fig. 3), the streamline starting at different lateral positions encounter the third and the fourth shock at different locations. For this region, the friction over a unit width is first calculated along five different streamlines, and is integrated to evaluate the total friction over these panels using the Simpson's rule. Calculations showed that five streamlines lead to solutions that are accurate to within 0.1% compared to those solutions with nine streamlines.

For the contoured portion of the expansion, shown schematically in Fig. 6, accurate calculation of skin friction is difficult because the contours are unknown. Here, skin friction is assumed to be that of the four flat plates shown in Fig. 7. The lengths of these flat plates are arbitrarily assumed to be 3 m as shown. The inaccuracies in computing the skin friction drag do not impact the conclusion regarding which design, MHD or non-MHD, generates higher specific impulse, since drag in both cases is computed in the same manner.

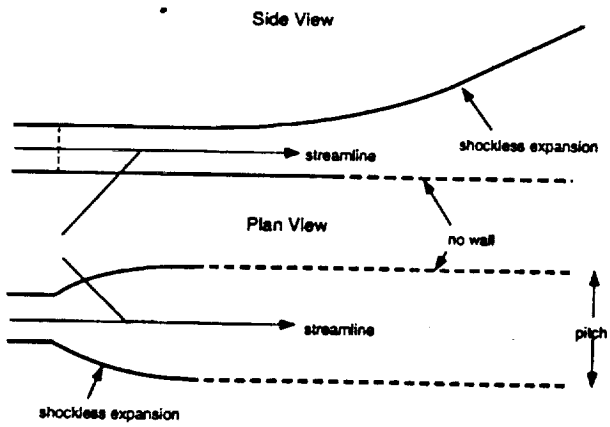

Figure 6. Schematic of the transition from the MHD accelerator to one-sided expansion.

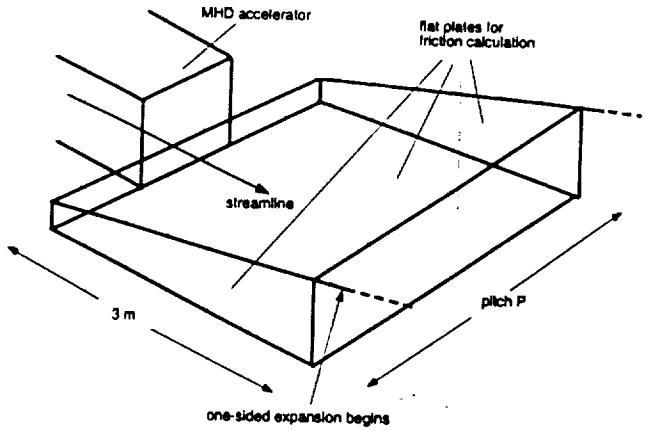

Figure 7. Flat plates assumed for friction calculation of the contoured expansion region.

Highest Specific Impulse

The combustor entrance Mach number M_c is varied as 1.5, 2.0, and 2.5, which are within the realistic range of possibilities for a scramjet combustor. The vehicle height H is varied as 3.5, 4, 4.5, 5, and 5.5 m, although most of the results are for 3.5 m. The load factor pair, α_1 - α_2, is varied as 0.95-1/0.95, 0.90-1/0.90, and 0.80-1/0.80. The fuel equivalence ratio is kept at unity for all cases, and the flight dynamic pressure is kept at 1 atm.

For a flight speed V, the combustor entrance Mach number M_c, the vehicle height H, and the seed substance and seed mass fraction chosen, one can vary the ramp angle θ arbitrarily. The resulting specific impulse value is a function of the ramp angle. Calculation is performed at an interval in θ of 0.1° to first produce a table of specific impulse versus θ. The ramp angle giving the highest specific impulse is chosen from this table as the optimum ramp angle for that condition.

The thrust is calculated as the difference between the outgoing (at the tail of the vehicle) and incoming momenta (at the nose of the vehicle). Specific impulse is calculated by dividing this thrust by the sum of the flow rates of the fuel and the seed material.

Results

General Features of Solutions

In Fig. 8, the specific impulses obtained by the present method are compared with those obtained by the sudden-freezing approximation used in Refs. 4 and 5, for the single-plane four-ramp compression system considered therein. The combustor entrance Mach number M_c was 2 for this case. Skin friction drag is not included in this comparison. As seen in Fig. 8, there is only a small difference between the kinetic and sudden-freezing calculations.

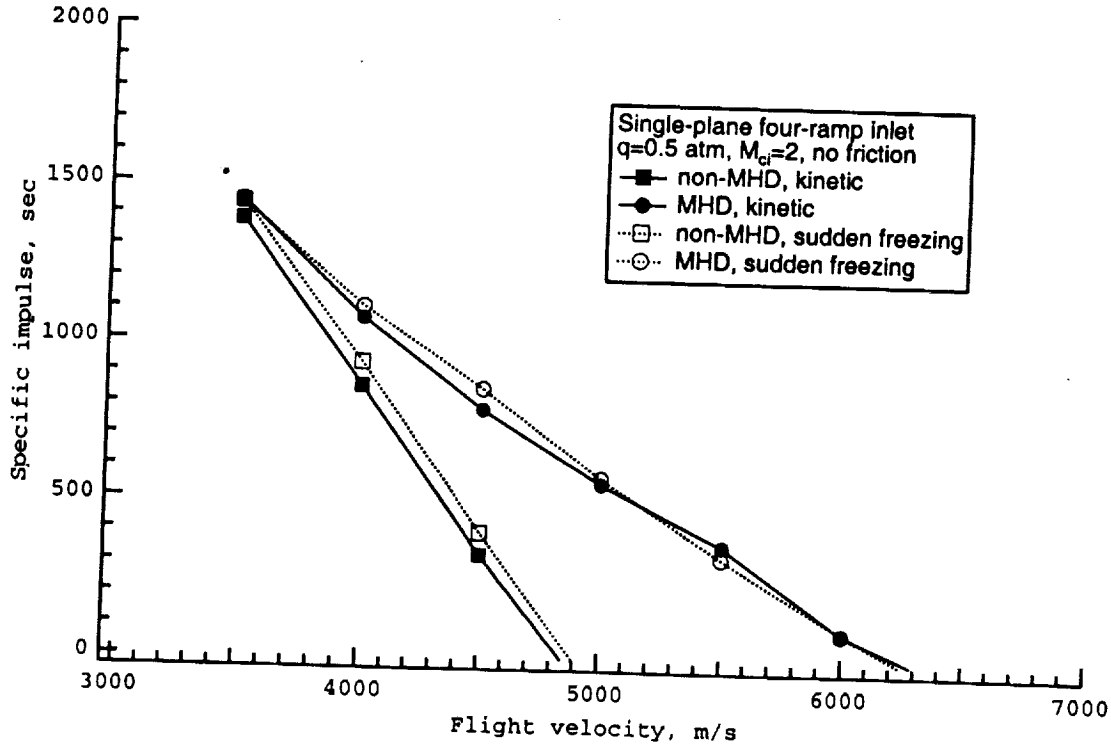

Figure 8. Comparison of the specific impulse obtained by kinetic calculation and that with the sudden-freezing calculation; $\alpha_1 = 0.95$, $\alpha_2 = 1/0.95$; and potassium seed.

Compared with the single-plane four-ramp design of Ref. 4, the present two-plane four-ramp design generates a vehicle of a smaller height, H. As a result, the area ratio of nozzle expansion is slightly smaller than in the previous design. The length of the nozzle is affected by the height: the larger the height, the shorter becomes the nozzle. For the vehicle of H less than 5 m, the present nozzle is longer than that of the single-plane four-ramp design. As a result, for the present vehicles of H < 5 m, expansion becomes more gradual than for the single-plane four-ramp design. This gradual expansion results in a nozzle flow closer in chemical equilibrium at the exit. This in turn produces a greater thrust. However, the longer nozzle also produces greater friction drag. Thus the functional relationship between the height H and specific impulse becomes somewhat complicated.

In Fig. 9, the optimum vehicle geometry is compared between typical MHD and non-MHD cases with friction and with finite-rate chemistry in the nozzle. For this case, V = 3.75 km/s, α_1 and α_2 are 0.95 and 1/0.95, M_c = 1.5, and H = 3.5 m. As indicated, the optimum angle of the ramps for the MHD and the non-MHD cases are θ = 16.5 and 25.6°, respectively. As has been pointed out in Ref. 4, this difference in the optimum θ occurs because of the constraint on M_c.

The pressure distribution along the flow path for these two vehicles is compared in Fig. 10. As shown here, because of the large θ, the non-MHD vehicle is subject to a higher pressure in the inlet region than the MHD vehicle. This causes larger form drag for the non-MHD vehicle. The specific impulses for these two cases are 791.7 sec for the MHD vehicle and 704.7 sec for the non-MHD vehicle.

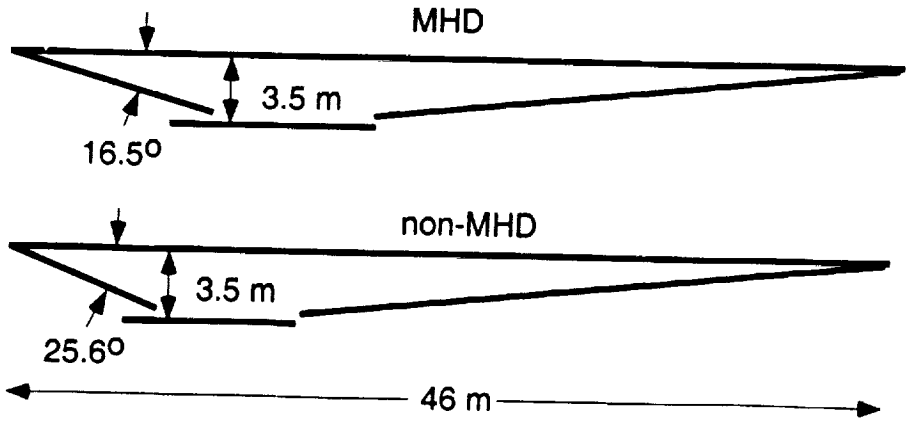

Figure 9. Comparison of the optimum configuration between the MHD and the non-MHD vehicles. V = 3.75 km/s, M_c = 1.5, H = 3.5 m, α_1 = 0.95, α_2 = 1/0.95, potassium seed.

The friction drag per meter of the vehicle width to the two vehicles are shown by components in Figs. 11(a) and (b). Because θ is different between the two vehicles, the friction drag values are slightly different on the three ramps. The friction drag for these ramps is slightly larger for the MHD case because the MHD case produces longer ramps. The sum of the drags by the MHD generator, fuel injector, and the MHD accelerator for the MHD vehicle, shown in Fig. 11(b), is lower than the sum of the drags by the isolator and the combustor for the non-MHD vehicle shown in Fig. 11(a).

The details of a typical solution for a two-plane four-ramp compression design are given in Table 2. The highlights of this solution are that: (1) the height is 3.5 m, the ramp angle is 16.5°, and the pitch is 1.842 m; (2) the vehicle produces 43 tons of thrust per 1 meter of vehicle width and a specific impulse of 791.7 sec (as opposed to 704.7 sec for the non-MHD vehicle); (3) the load factors α_1 and α_2 are 0.95 and 1/0.95, respectively, (4) the magnetic fields required for the MHD generator and accelerator are 11.29 and 9.115 Tesla, respectively; and (5) the axial voltage gradient, which must be below about 5000 V/m (see Ref. 4), is below 4425 V/m.

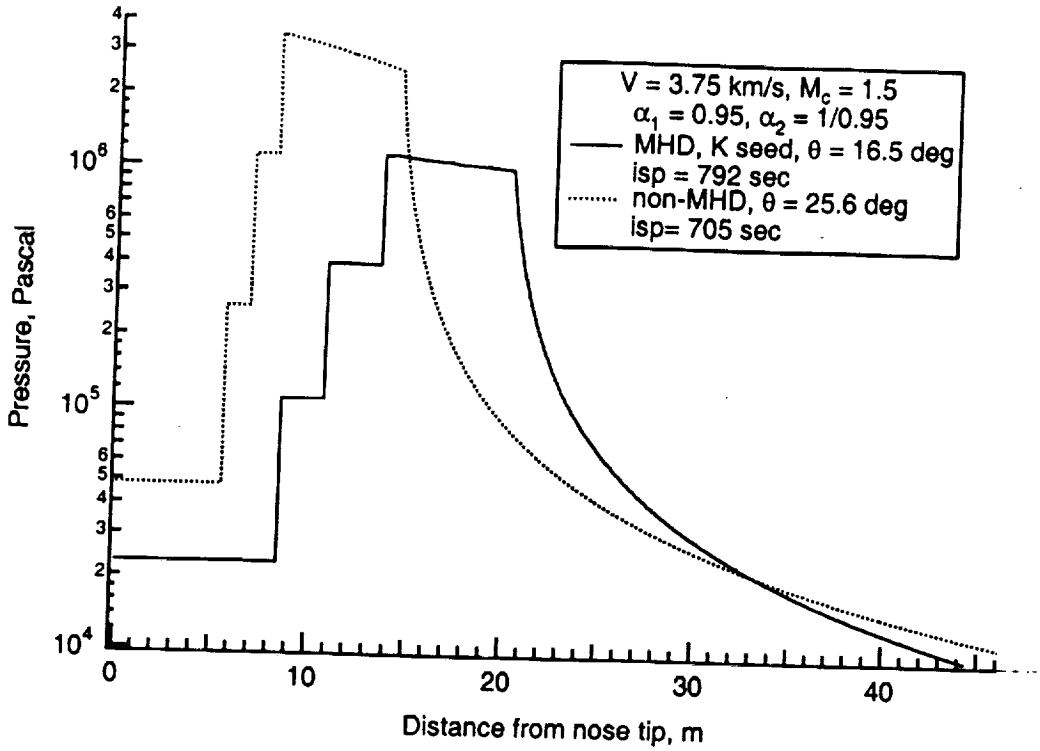

Figure 10. Comparison of static pressure distribution over the MHD and the non-MHD vehicles with friction and finite-rate chemistry in the nozzle. V = 3.75 km/s, M_c = 1.5, H = 3.5 m, α_1 = 0.95, α_2 = 1/0.95.

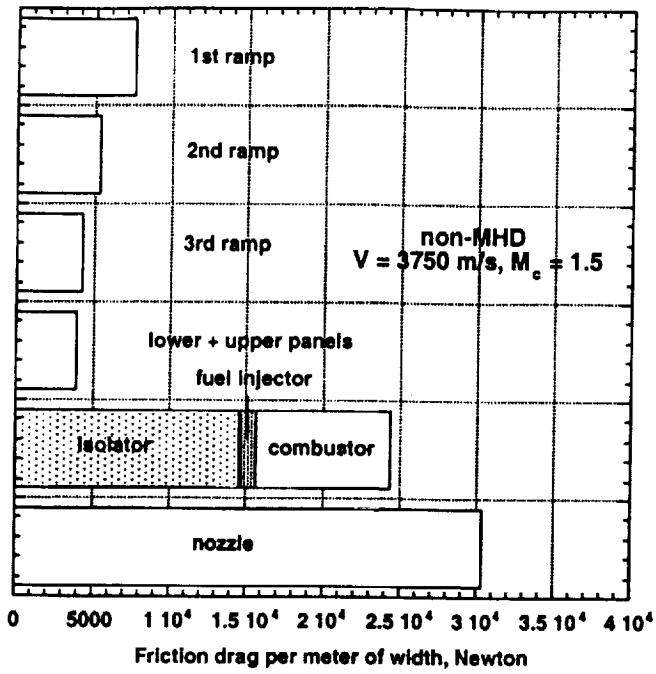

Figure 11. Breakdown of friction drag per 1 m of vehicle width; V = 3750 m/s, M_c = 1.5, H = 3.5 m. (a) non-MHD vehicle.

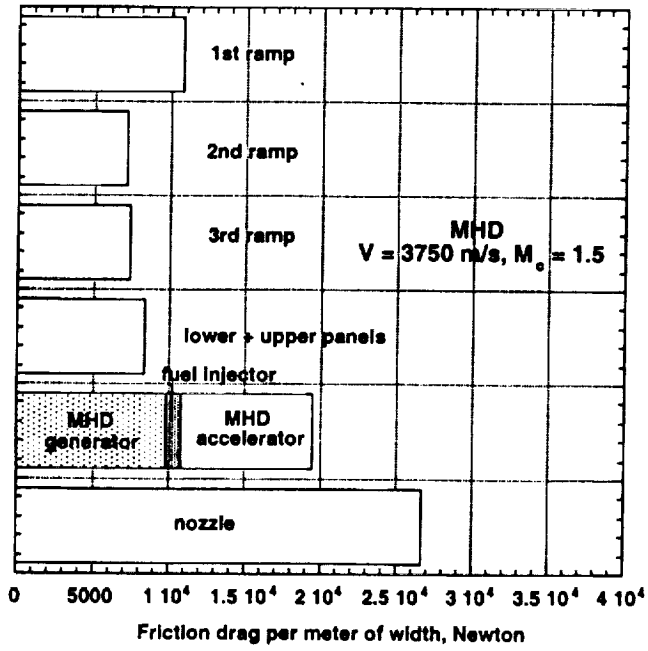

Figure 11(b). MHD vehicle; $\alpha_1 = 0.95$, $\alpha_2 = 1/0.95$; potassium seed.

Table 2. Summary of a typical solution.

Freestream	
Flight speed	3.75 km/s
Flight dynamic pressure	1 atm (2116 psf)
	(1.014×10^5 Pascal)
Mach number	11.81
Freestream temperature	250 K
Freestream density	1.441×10^{-2} kg/m^3
Freestream pressure	1.039×10^3 Pascal
Number of ramps	4
Ramp angles	16.5°
Over 1st ramp	
Pressure	2.303×10^4 Pascal
Temperature	1378 K
Velocity	3487 m/s
Mach number	4.674
Pitch	1.842 m
Over 2nd ramp	
Pressure	1.095×10^5 Pascal
Temperature	2145 K
Velocity	3190 m/s
Mach number	4.048
Over 3rd ramp	
Pressure	3.954×10^5 Pascal

Temperature	2848 K
Velocity	3154 m/s
Mach number	3.451

Over 4th ramp (=entrance to seeder)

Pressure	1.113×10^{6} Pascal
Temperature	3397 K
Velocity	2792 m/s
Mach number	2.768
Capture air flow rate	189.15 kg/s
Enthalpy flow	1.565×10^{9} W/m

Seeding

Entrance height/width	33.50 cm
Overall inlet area ratio	51.96
Seeding material	potassium
Seed mass fraction	10^{-3}
Seed flow rate	0.189 kg/s
Pressure	1.116×10^{6} Pascal
Temperature	3397 K
Ionization mol fraction	4.431×10^{-5}
Electrical conductivity	33.25 mho/m

Entrance to MHD generator

Height/Width of channel	33.50 cm
Magnetic field	11.29 Tesla
Hall parameter	2.808
Transverse voltage gradient	-29,920 V/m
Axial voltage gradient	4421 V/m
Voltage across electodes	10020 V

Current density	-5.236×10^4 A/m^2
Pressure	1.116×10^6 Pascal
Temperature	3397 K
Velocity	2789 m/s
Mach number	2.764
Enthalpy flow	1.676×10^9 W/m

At exit of MHD generator

Magnetic field	11.29 Tesla
Hall parameter	2.970
Transverse voltage gradient	-16,140 V/m
Axial voltage gradient	2523 V/m
Voltage across electrodes	7572 V
Current density	-2.876×10^4 A/m^2
Height/Width of channel	46.91 cm
Pressure	1.054×10^6 Pascal
Temperature	3393 K
Velocity	1505 m/s
Mach number	1 492
Length of generator	2.721 m
Enthalpy flow	1.043×10^9 W/m
Power extracted	5.220×10^8 W/m

At entrance to combustor

Equivalence ratio	1
Fuel flow rate	5.553 kg/s
Height/Width of channel	46.91 cm
Pressure	1.054×10^6 Pascal
Temperature	3393 K

Velocity	1505 m/s
Mach number	1.492
Fuel injector	
Fuel	gaseous hydrogen
Total temperature	500 K
Total pressure	2×10^7 Pascal
Nozzle exit velocity	2865 m/s
Nozzle exit static pressure	1.054×10^6 Pascal
At exit of injector section	
Pressure	1.035×10^6 Pascal
Temperature	3518 K
Velocity	1555 m/s
Mach number	1.327
Enthalpy flow	1.082×10^9 W/m
At entrance to MHD accelerator	
Magnetic field	9.115 Tesla
Hall parameter	2.212
Transverse voltage gradient	14,920 V/m
Axial voltage gradient	1650 V/m
Voltage across electrodes	8129 V
Current density	2.597×10^4 A/m^2
Height/Width of channel	54.49 cm
Pressure	1.035×10^6 Pascal
Temperature	3518 K
Velocity	1555 m/s
Mach number	1.327
Ionization fraction	5.302×10^{-5}

Electrical conductivity	34.82 mho/m
Enthalpy flow	1.080×10^9 W/m

At exit of MHD accelerator (=entrance to nozzle)

Magnetic field	9.115 Tesla
Hall parameter	1.317
Transverse voltage gradient	26,970 V/m
Axial voltage gradient	3124 V/m
Voltage across electrodes	11,190 V
Current density	4.724×10^4 A/m^2
Height/Width of channel	41.49 cm
Pressure	9.859×10^5 Pascal
Temperature	3502 K
Velocity	2811 m/s
Mach number	2.400
Length of accelerator	2.846 m
Enthalpy flow	1.612×10^9 W/m
Power consumed	5.334×10^8 W/m

At nozzle exit

Area ratio	37.7
Pressure	9.173×10^3 Pascal
Temperature	1951 K
Velocity	4124 m/s
Enthalpy flow	1.604×10^9 W/m
Mach number	4.441

Overall performance

Energy bypass ratio	0.3336
Net thrust	4.311×10^4 N

Seed + fuel flow rate	5.553 kg/s
Specific impulse	791.7 sec

Parametric Study

In Fig. 12, the calculated specific impulse values for M_c = 1.5 are compared between the MHD case with potassium seeding and cesium seeding and with α_1 =0.95 and α_2 = 1/0.95, the non-MHD case, and a typical rocket (with specific impulse of 450 sec). The plotted "with friction" values are obtained by choosing the ramp-angle θ that maximizes the specific impulse while including friction in the thrust calculation. That is, the design is optimized including friction. The "without friction" values plotted are obtained by removing friction from the thrust calculation for the same vehicle at the same flight condition. The "without friction" values are therefore not of the optimized vehicles.

As seen in Fig. 12, the skin friction for fully turbulent flow greatly reduces the specific impulse. The two MHD cases produce higher specific impulses than the non-MHD case between the flight speeds of 3400 and 4000 m/s. Potassium seeding gives about the same specific impulse as cesium seeding. Compared with the single-plane four-ramp results shown in Fig. 8, the present results show higher specific impulses when friction is ignored ("without friction" values). This is a result of the gradual expansion in the nozzle mentioned earlier.

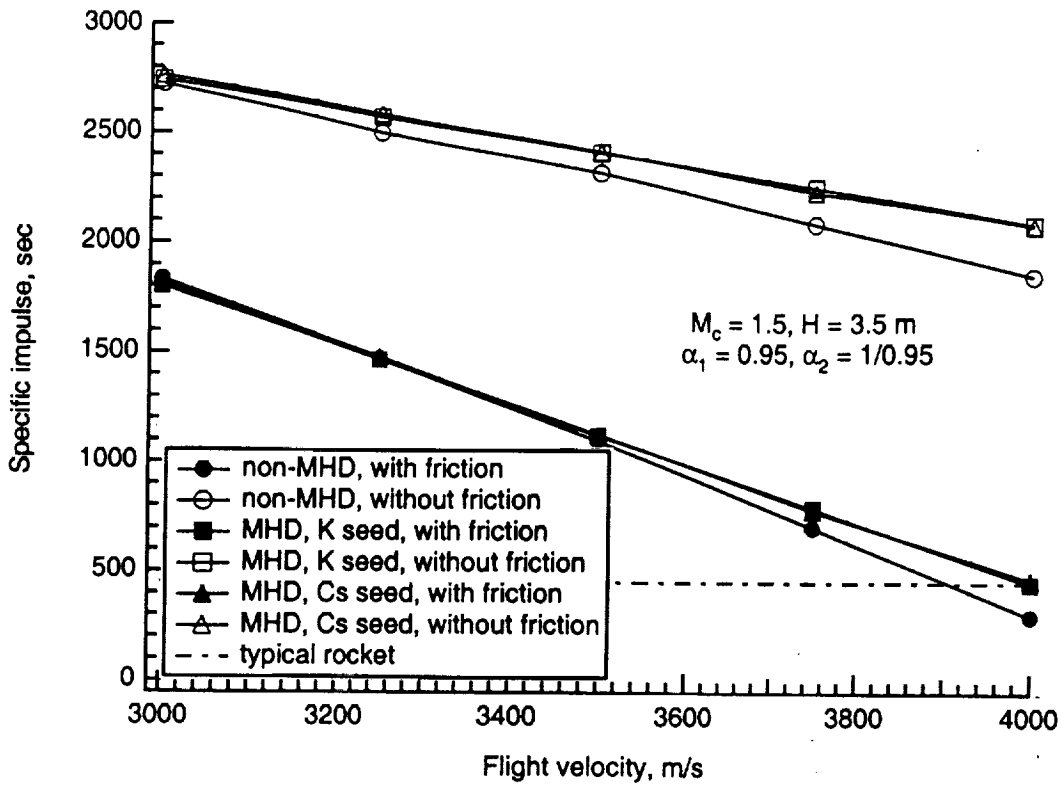

Figure 12. Comparison of specific impulse with friction between the MHD case with potassium and cesium seed and the non-MHD case. M_c = 1.5, α_1 = 0.95,α_2 = 1/0.95, and H = 3.5 m.

The effect of changing the combustor entrance Mach number M_c on specific impulse is studied in Fig. 13. As seen here, the case of M_c = 1.5 with MHD yields higher specific impulses than the non-MHD case at flight speeds above 3400 m/s. At M_c greater than 1.5, the MHD cases give specific impulses equal to or lower than the non-MHD case.

The effect of the load factors α_1 and α_2 on specific impulse is studied in Figs. 14(a) to (c). Specific impulse deteriorates with α_1 and α_2 deviating farther away from unity.

The impact of varying vehicle height H on specific impulse is shown in Fig. 15 for V = 3.75 km/s and M_c = 1.5. By increasing H, the specific impulse of the MHD-bypass vehicle is increased. The specific impulse for the non-MHD vehicle also increases slightly more. As a result, for this condition the advantage of the MHD-bypass system decreases at large H.

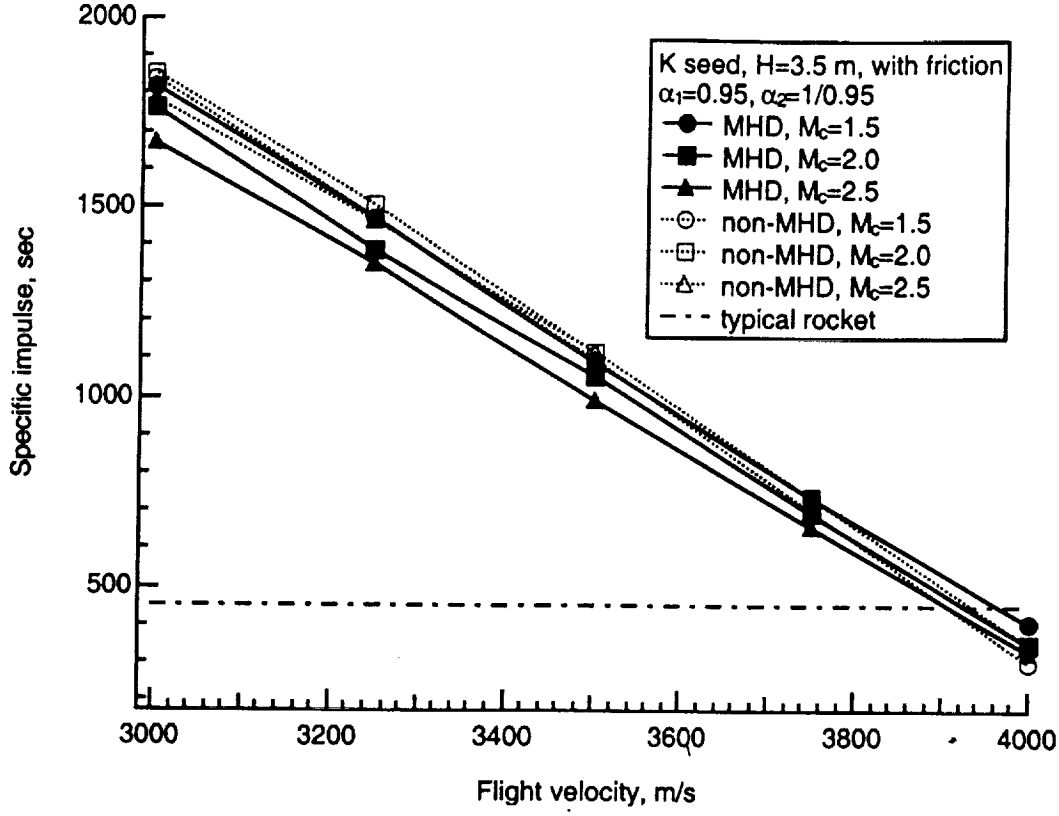

Figure 13. Effect of combustor entrance Mach number, M_c

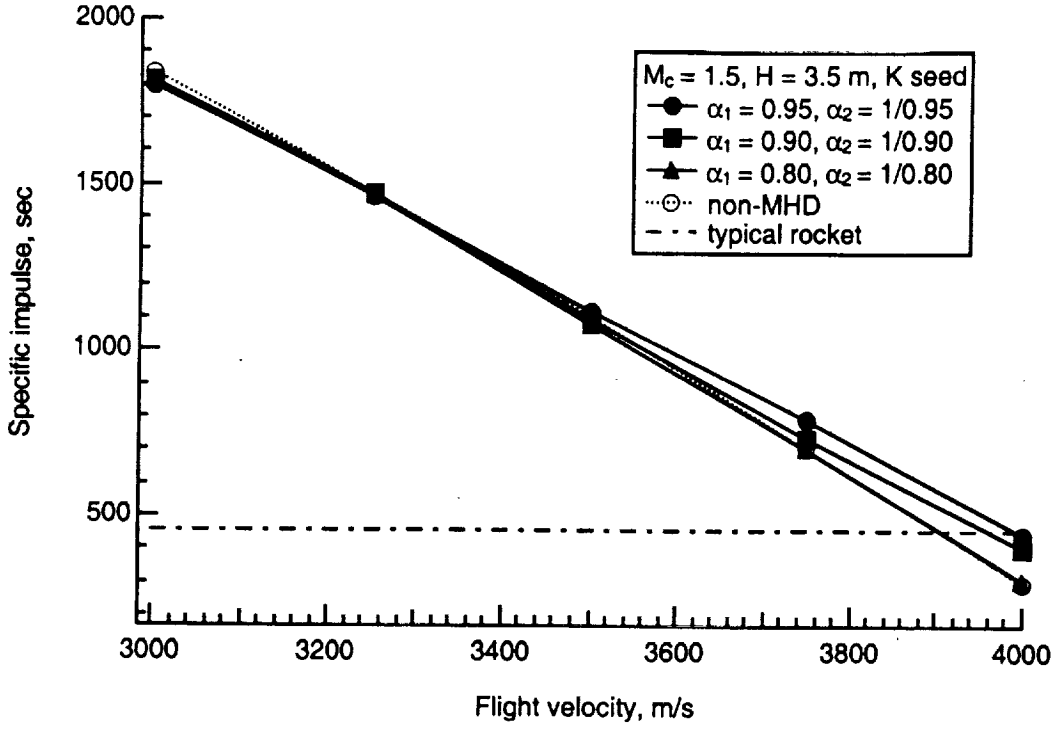

Figure 14. Effect of load factors α_1 and α_2 on specific impulse. (a) M_c = 1.5.

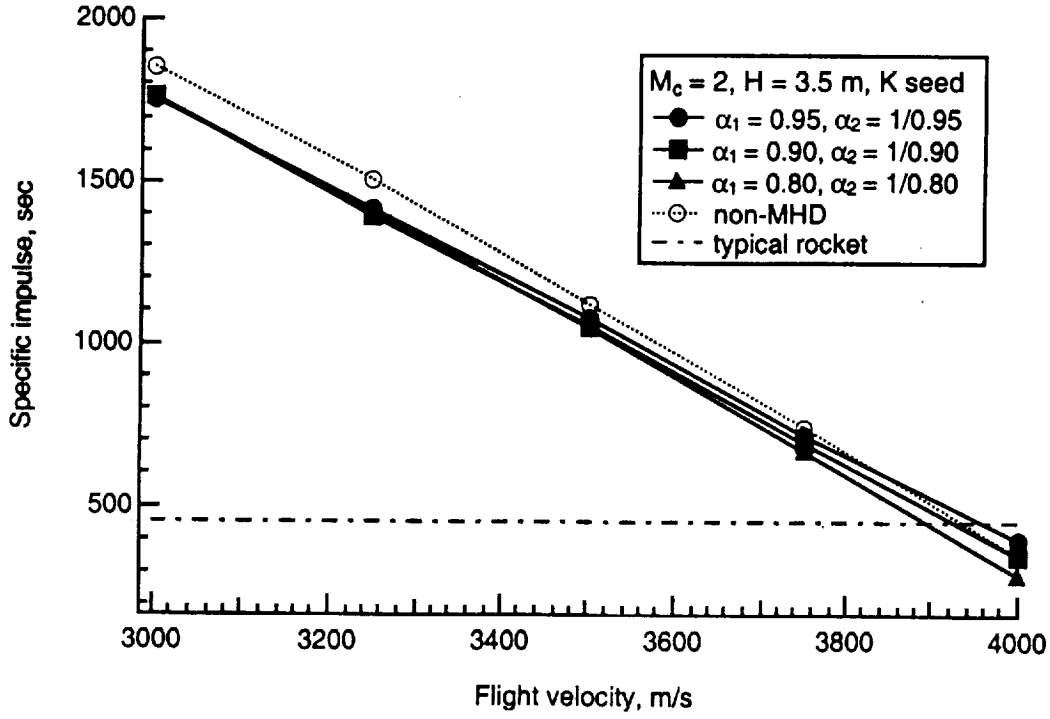

Figure 14(b). $M_c = 2.0$.

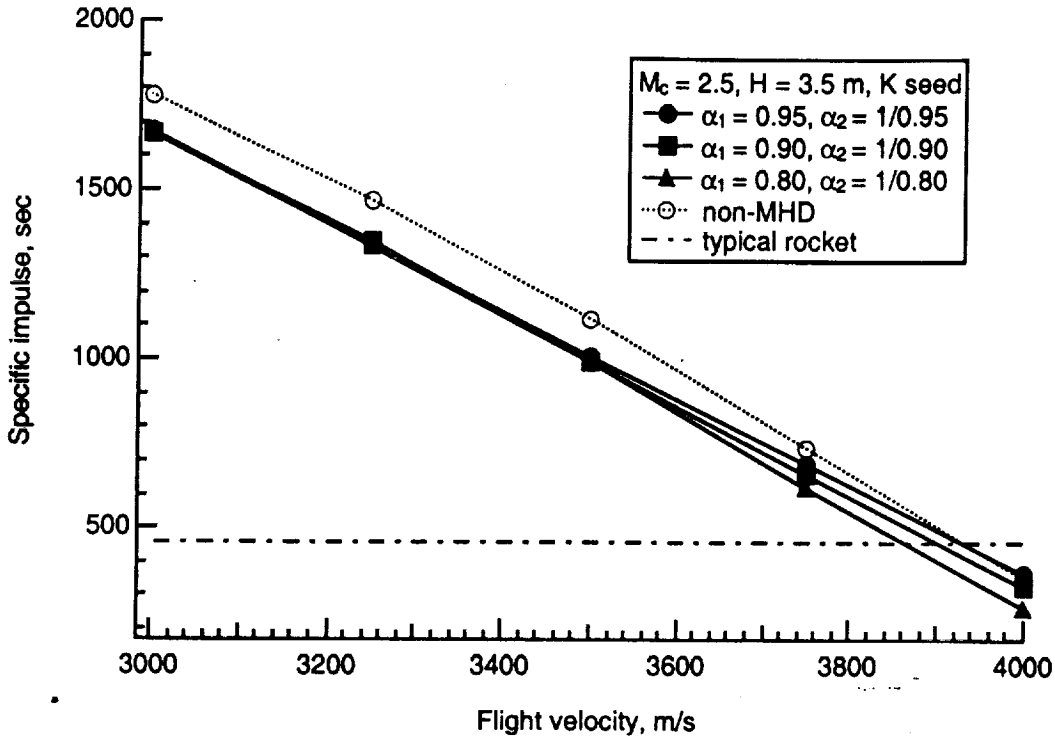

Figure 14(c). $M_c = 2.5$.

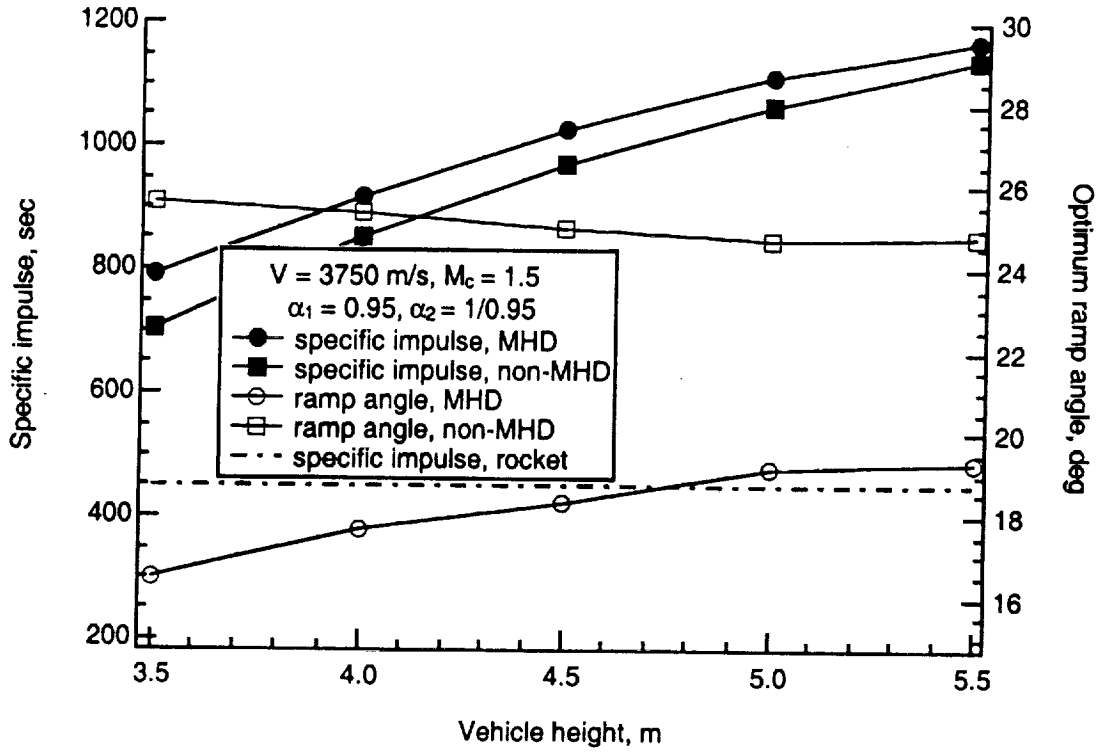

Figure 15. Impact of vehicle height H on specific impulse.

The optimum geometry of the present two-plane four-ramp compression design is one in which the reactor is located close to the leading edge, as shown in Fig. 9. The location of the reactor can be moved aft by increasing the ramp angle of the third and fourth ramps. Calculation was performed with the angle of the third (and fourth) ramp that is 1.5, 2, and 2.5 times the angle of the first (and the second) ramp. The overall length of the vehicle is kept the same. In Fig. 16, the result of that calculation is shown. As the figure shows, increasing the third/fourth ramp angle can increase the distance from the vehicle leading edge to the reactor entrance. However, specific impulse is decreased significantly due to increased total pressure losses at the two stronger shocks.

Discussion

In Ref. 4, a method was presented for assessing the theoretical performance of an MHD-energy bypass scramjet propulsion system under several simplifying assumptions. In the present work, this method of performance calculation is improved by eliminating two key assumptions. The flow is taken to be viscous, and the chemical reactions occur at a finite rate. The improved method provides a more realistic assessment of this propulsion concept than the previous method did.

In the present work, the boundary layer in the flow path is assumed to be fully turbulent starting from the leading edge. The boundary layer over the first ramp and the second ramp are no doubt at least partly laminar. Consideration of laminar boundary layer over these two components will lower the skin friction values for these two components. However, according to Figs. 11(a) and (b), the contribution of these two components to the total drag is relatively small. The end result is that the inclusion of viscous friction lowers specific impulse substantially.

With the present design, the MHD-bypass system produces specific impulses that are better than those for the non-MHD scramjet system and for a typical rocket engine between the flight velocity of 3400 and 4000 m/s. Over a narrow range of design parameters, namely, for combustor entrance Mach number of 1.5, the vehicle height smaller than 4 m for a 46 m long vehicle, the MHD-bypass system has an advantage over the non-MHD system. At the flight velocity of 3900 m/s with M_e = 1.5, the specific impulse for the MHD case exceeds that of the non-MHD case ant that of the typical rocket by about 150 secs. At this condition, the MHD-bypass system offers a clear advantage over the non-MHD case for hypersonic cruiser application.

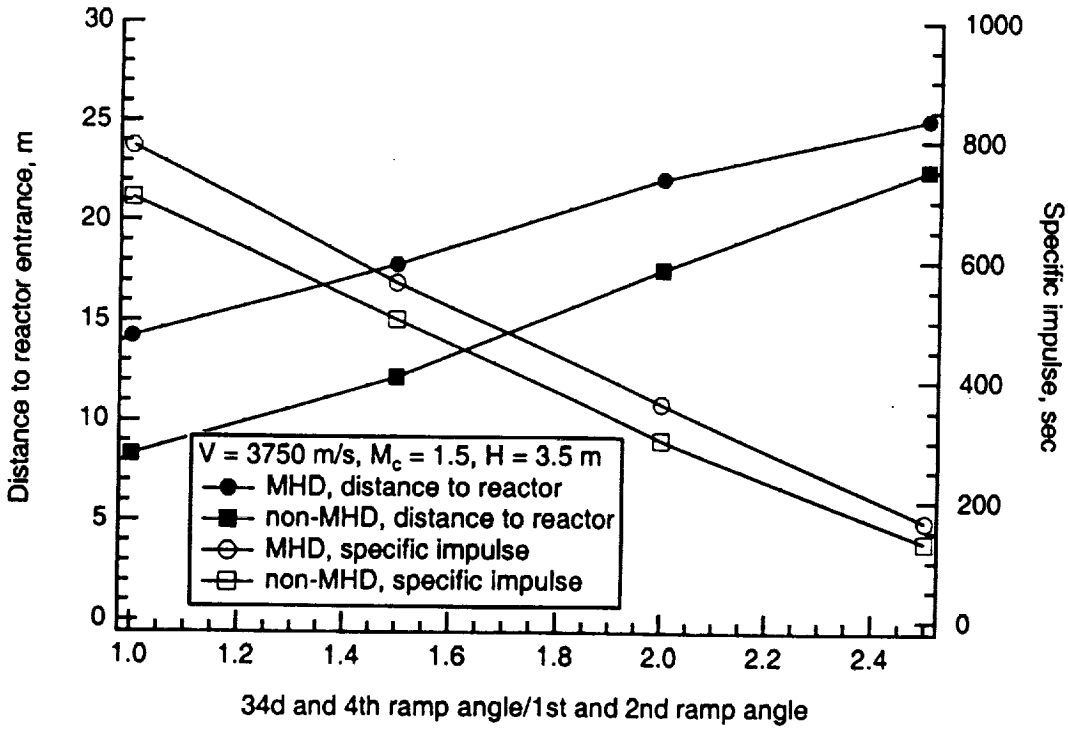

Figure 16. Effect of changing the ratio of the third and fourth ramp angles to the first and second ramp angles.

As seen above, the present two-plane four-ramp compression design is superior to the single-plane four-ramp design in Ref. 4. With the present design, performance is seen to be a complex function of the ramp angles and vehicle height. In reality, portion of compression will be by an isentropic compression instead of shock compression. When isentropic compression is introduced into the design, performance will be an even more complex function of geometry. This offers hopes for further improving the performance of the MHD-energy bypass scramjet system.

In reality, it is probably rather difficult to realize some of the assumptions made for the MHD-system. First, the computed results for magnetic field in the magnetic devices are quite high. These values are currently not feasible for the spaceliner application. Second, the skin friction through the MHD devices may be larger than that for the non-MHD system, because the MHD devices have electrodes which produces effectively a rough surface. Third, equilibrium ionization with seeding requires temperatures greater than

3000° K, presenting a challenge for designing an appropriate thermal management system and for developing appropriate thermal protection system including ultra-high-temperature and light-weight materials. Fourth, three-dimensional simulations are essential for fully accounting the effects of the electric and magnetic fields on the propulsive flow field. Fifth, specific impulse of airbreathing hypersonic propulsion system is very sensitive to vehicle design and operation.

At moderate hypersonic flight Mach numbers, the energy management with MHD principles facilitates operation of scramjet as if it is operated at low hypersonic flight Mach numbers. A great deal of research and development would seem necessary for the MHD devices to function as efficiently as assumed. The viability of energy management with MHD devices needs to be determined by conducting conceptual designs of realistic spaceliners with MHD energy bypass scramjets and assessments of vehicle performance using analysis methods with further improvements.

Conclusions

The energy management with MHD offers the possibility of enhancing the performance of scramjet. An MHD-energy bypass scramjet with a two-plane four-ramp inlet geometry has a higher thrust performance than one with a single-plane four-ramp inlet geometry. If the boundary layer of the flow in the propulsive flowpath for the MHD-energy bypass scramjet propulsion system is fully turbulent, if the length of the reactor for the MHD-system (MHD generator + fuel injector + MHD accelerator) is the same as that of the non-MHD scramjet system, and when the height-to-length ratio of the vehicle is limited to below a certain value, then the specific impulse of the MHD system is slightly greater than that of the non-MHD system and a typical rocket within a speed range between 3400 and 4000 m/s. The specific impulse of the MHD system is nearly 150 sec higher than that of the non-MHD system and that of a typical rocket systems at 3900 m/s. At this speed, the MHD system offers an advantage over the non-MHD system for the hypersonic cruiser application. At flight speeds higher than 4000 m/s, the MHD-system is better than the non-MHD system, but the absolute value of specific impulse is below that of a typical rocket.

Specific impulse is a complex function of geometry; by varying geometry and by improving the analysis method, further improvements in performance may be possible. A system analysis of a realistic spaceliner with MHD-bypass scramjet is recommended to assess the viability of this propulsion concept. Major research and technology issues are identified.

Acknowledgement

C. Park and D. Bogdanoff wish to acknowledge the support provided by NASA Ames Research Center through contract NAS2-99092 to ELORET Corporation. The similar results presented in "Real-Gas Calculation of MHD-Bypass Scramjet Performance" (AIAA Paper 2000-3702, 36th AIAA/ASME/SAE/ASEE Joint Propulsion Conference & Exhibit, Huntsville, AL, 16-19 July 2000) for the scramjet vehicle employing two-plane four-ramp inlet system were found to contain computational errors. That paper should be disregarded.

References

[1]Novichov, N. "Space Wings of Russia and the Ukraine," *Echo of the Planes/Aerospace*, Moscow, September 1990.

[2]Gurijanov, E.P. and Harsha, P. T., "AJAX: New Directions in Hypersonic Technology," AIAA Paper 96-4609, 1996.

[3]Bityurin, V. A., Lineberry, J. T., Potebnia, V. G., Alferov, V. I., Kuranov, A. L., and Sheikin, E. G., "Assessment of Hypersonic MHD Concepts," AIAA Paper 97-2393, June 1997.

[4]Park, C., Bogdanoff, D. W., and Mehta, U. B, "Theoretical Performance of MHD-Bypass scramjet," paper presented at Joint Meeting of the Combustion Subcommittee, Airbreathing Propulsion Subcommittee,

Propulsion Systems and Hazards Subcommittee of JANNAF, October 18-22, 1999; to appear in *Journal of Propulsion and Power.*

[5]Chase, R. L., Mehta, U. B., Bogdanoff, D. W., Park, C., Lawrence, S., and Aftosmis, M., "Comments on an MHD Energy Bypass Engine Powered Spaceliner," AIAA Paper 99-4965, November, 1999.

[6]Park, C., *Nonequilibrium Hypersonic Aerothermodynamics*, John Wiley and Sons, New York, N. Y., 1990, p. 267.

[7]Baulch, D. L., Drysdale, D. D., and Horne, D. G., *Evaluated Kinetic Data for High Temperature Reactions*, CRC Press, 1972.

[8]NASP High Speed Propulsion Technology Team, "Hypersonic Combustion Kinetics," Status Report of the Rate Constant Committee, December 1989.

[9]Bose, D. and Candler, G. V., "Thermal Rate Constants of the $N_2 + O \rightarrow NO + N$ Reaction Using ab initio $^3A''$ and $^3A'$ Potential Energy Surfaces," *Journal of Chemical Physics*, Vol. 104, No. 8, February 1996, pp. 2825-2833.

[10]Van Driest, E. R., ""Turbulent Boundary Layer in Compressible Fluids," *Journal of the Aeronautical Sciences*, Vol. 18, No. 3, March 1951, pp. 145-160.

[11]Hopkins, E. J., "Charts for predicting Turbulent Skin Friction From the Van Driest Method (II)," NASA TN D-6945, October 1972.